Magnetic Fields of a Dipole in Special Volume Conductor Shapes

B. NEIL CUFFIN, MEMBER, IEEE, AND DAVID COHEN, SENIOR MEMBER, IEEE

Abstract—Expressions are presented for the magnetic fields produced by current dipoles in four basic volume conductor shapes. These shapes are the semi-infinite volume, the sphere, the prolate spheroid (egg-shape), and the oblate spheroid (discus-shape). The latter three shapes approximate the shape of the human head and can serve as a basis for understanding the measurements of the brain's magnetic fields. The semi-infinite volume is included in order to investigate the effect of the simplest boundary between a conductor and nonconductor. The expressions for the fields are presented in a form which separates the total field into two parts. One part is due to the dipole alone (the dipole field); the other is due to the current generated in the volume conductor by the dipole (the volume current field). Representative plots of the total field and the volume current field are presented for each shape. The results show that for these shapes the component of the total field normal to the surface of the volume conductor is produced completely or in large part by the dipole alone. Therefore, measurement and use of this component will greatly reduce the complexity of determining the sources of electrical activity inside a body from measurements outside the body by removing the necessity of dealing with the volume current field.

INTRODUCTION

IN RECENT YEARS, measurements of the magnetic fields produced by the human heart (the magnetocardiogram or MCG) and brain (the magnetoencephalogram or MEG) have been made in order to obtain information about the electrical activity of these organs [1]-[6]. In addition, several digital computer studies using realistic heart and torso models have been performed in order to investigate the MCG [7]-[9]. The ultimate goal of this work is the solution of the inverse problem of magnetic measurements, i.e., the determination of the nature and location of electrical activity inside the body from measurements outside the body. As is the case with the inverse problem for measurements of electric potentials on the body surface, the solution of the magnetic inverse problem is greatly complicated by individual variations in anatomy. However, some understanding of the magnetic fields produced by these organs and their use in the solution of the inverse problem can be obtained from a study of the fields produced by dipoles in volume conductors with elementary shapes. For example, some recent experimental work [10] dealing with a dipole in a semi-infinite volume has shown that the component of the field normal to the surface can be considered to be produced by the dipole alone; the current in the volume conductor generated by the dipole contributes nothing to this component of the field. For this case, measurements of the normal component of the field obtain information about the field produced by the dipole only without any interference from the volume current; the complexity of the inverse problem is thereby reduced.

This result suggests the convenient method of considering the total magnetic field, $\bar{H}$, as being the sum of the magnetic field produced by the dipole alone, $\bar{H}_d$, plus the magnetic field produced by the current flowing in the volume conductor, $\bar{H}_v$. This division of the field into two parts is particularly useful when considering the actual physical situation since $\bar{H}_d$ is associated with the generators in the active nerve or muscle tissue, while $\bar{H}_v$ is associated with the current flowing in the body which is produced by these generators. If conditions for which a component of $\bar{H}_v$ is negligible compared to the same component of $\bar{H}_d$ can be found for the body, then measurements of this component over the body surface will obtain information about the electrical activity of nerve or muscle tissue inside the body with negligible interference from the current flowing in the rest of the body. The first step in determining these conditions for the body must proceed from a study of the magnetic fields produced by dipoles in elementary volume conductor shapes.

In addition, the magnetic fields produced by dipoles in elementary volume conductor shapes can be useful in understanding the fields measured near the body in another way. A comparison of elementary volume conductor fields with the body's fields may lead directly to insights into the location of the electrical activity inside the body. For example, comparing the field produced by a dipole in a sphere with the field measured near the head may suggest areas of electrical activity in the brain.

In this paper, four elementary volume conductor shapes are considered; three of these shapes approximate the shape of the human head and are therefore useful in analyzing the MEG. The four shapes are the semi-infinite volume, the sphere, the prolate spheroid, and the oblate spheroid. The semi-infinite volume is obviously a rather poor approximation to the shape of the head, but it is included since it provides the means to study the effect of the simplest boundary between a conductor and nonconductor. Expressions for the magnetic fields produced by dipoles in the four shapes are presented in a form which separates $\bar{H}$ into the two parts $\bar{H}_d$ and $\bar{H}_v$. Study of the ratios of the components of $\bar{H}_d$ and $\bar{H}$ for each shape points out those conditions for which a component of $\bar{H}_v$ is negligible compared to the same component of $\bar{H}_d$. In addition, representative plots of $\bar{H}$ and $\bar{H}_v$ are presented for each shape. On the basis of the expressions and plots, it is found that for all four shapes the component of $\bar{H}$ normal to the surface is the one which has the minimum $\bar{H}_v$ contribution.

Manuscript received December 29, 1975; revised July 22, 1976. This work was supported by the Advanced Research Projects Agency under subcontract on ONR Contract N00014-70-C-0350.

The authors are with the Francis Bitter National Magnet Laboratory, Massachusetts Institute of Technology, Cambridge, MA 02139.

Calculation of the Magnetic Fields

In this section, the expressions for the magnetic fields produced by dipoles in the four volume conductor shapes are developed. In this development, the total magnetic field is considered to be the sum of a dipole term plus a volume current term ($\bar{H} = \bar{H}_d + \bar{H}_v$). The expressions are used to calculate and plot $\bar{H}$ and $\bar{H}_v$ in some representative planes. Also methods of determining the ratios of the components of $\bar{H}_d$ and $\bar{H}$ are developed for each shape. The dipole will be considered to be a current dipole for which $\bar{H}_d$ can be calculated from the Biot-Savart law as

$$\bar{H}_d = \frac{\bar{P} \times \bar{R}}{4\pi R^3} \tag{1}$$

where $\bar{P}$ is the current dipole moment and $\bar{R}$ is a vector pointing from the location of $\bar{P}$ to the field point (point where the field is being calculated). The current dipole moment $\bar{P}$ is similar to a charge dipole moment except that its dimensions are current-length rather than charge-length.

In order to simplify the development, we state here symmetry conditions for which $\bar{H} = 0$: If a dipole is located on and oriented along the axis of a volume conductor having axial symmetry, then $\bar{H} = 0$ everywhere outside of the conductor. A simple example of these conditions is a radially oriented dipole in a sphere where analysis shows that $\bar{H} = 0$ outside of the sphere because of the symmetrical current distribution. A rigorous proof of the statement is provided by Grynszpan and Geselowitz [11].

Semi-Infinite Volume

For a dipole oriented normal to the surface of a semi-infinite volume conductor, $\bar{H} = 0$ in the nonconducting region due to the symmetry conditions discussed above. Therefore, only a dipole oriented tangential to the surface, as in Fig. 1A, need be considered. Since no currents are present in the nonconducting region, the scalar magnetic potential, φ, can be used to calculate the field in this region. Boundary conditions necessary and sufficient to obtain a unique solution for φ can be found by determining the normal derivative of φ on the surface, as this will define a Neumann boundary value problem. If

$$\bar{H} \equiv -\nabla\varphi \tag{2}$$

then

$$\left.\frac{\partial\varphi}{\partial z}\right|_{z=0} = -H_z\Big|_{z=0} \tag{3}$$

is the required boundary condition.

Since H_z is normal to the surface, it is produced by the dipole alone. One method of proving this is by considering the expression developed by Geselowitz [12] for $\bar{H}$ in the nonconducting region

$$\bar{H} = \frac{1}{4\pi}\iiint \bar{J}^i \times \nabla\left(\frac{1}{R}\right) dv + \frac{\sigma}{4\pi}\oiint V \nabla\left(\frac{1}{R}\right) \times \bar{ds} \tag{4}$$

where $\bar{J}^i$ is the current dipole moment per unit volume of the impressed or source current, σ is the conductivity of the medium, V is the electric potential on the surface of the volume conductor, and R is the distance from an element of volume dv or vector surface $\bar{ds}$ to the field point. The term containing the volume integral gives the $\bar{H}_d$ part of $\bar{H}$, while the term containing the surface integral gives the $\bar{H}_v$ part. For our purposes where discrete current dipoles are being considered, $\bar{J}^i\,dv$ becomes $\bar{P}$ and the contribution from the volume integral can be calculated using equation (1). For the geometry in Fig. 1A, it is evident that $H_{zv} = 0$ as a consequence of the cross-product in the surface integral. (H_{zv} indicates the z-component of $\bar{H}_v$. Similar double subscript notation will be employed in the rest of this development.) Therefore, at the surface $H_z = H_{zd}$, and it can be calculated from equation (1).

Using the boundary condition and the fact that $\nabla^2\varphi = 0$, the solution for φ is obtained as follows. Applying the technique

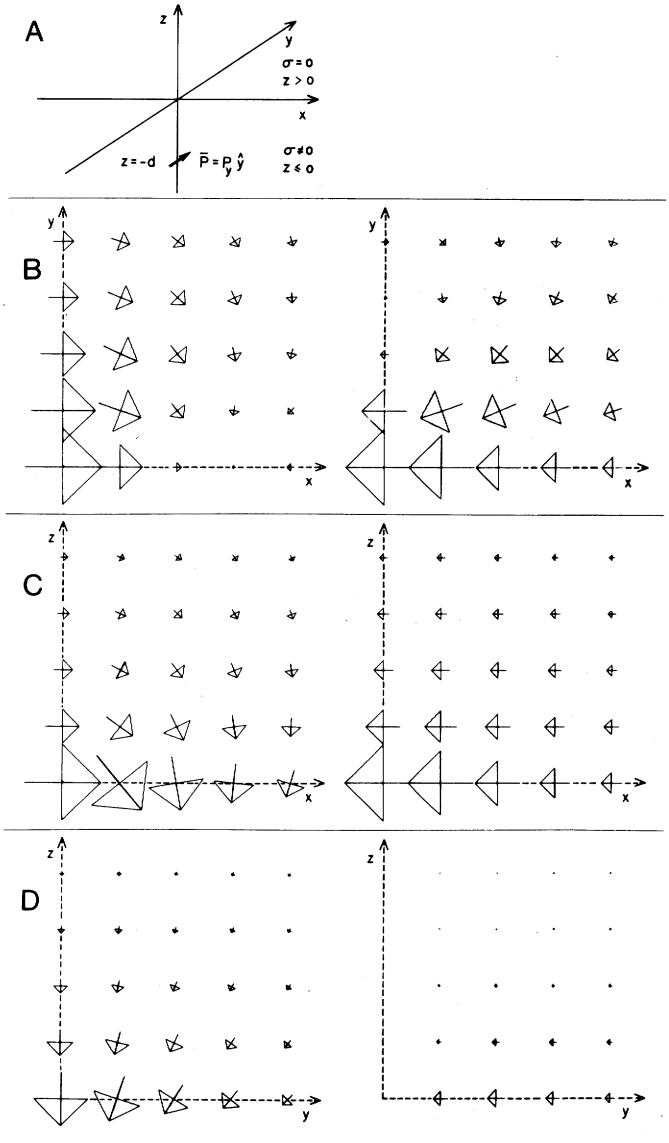

Fig. 1. Magnetic fields of a dipole in a semi-infinite volume. For the field plots, the arrows which are proportional to the components of the field (at the point where the tail of the arrow joins the head) are $d/2$ units apart. The scale is arbitrary but consistent for all plots in this figure. The plots on the left side are of $\bar{H}$; those on the right are of the corresponding $\bar{H}_v$. The fields are plotted in the following planes: (B) $z = 0$; (C) $y = 0$; and (D) $x = d$ (both $\bar{H}$ and $\bar{H}_v$ are normal to $x = 0$ plane).

of separation of variables, it can be shown that for $z > 0$

$$\varphi = \int_{-\infty}^{\infty}\int_{-\infty}^{\infty} G(\alpha,\beta)e^{j2\pi\alpha x}\, e^{j2\pi\beta y}\, e^{-2\pi(\alpha^2+\beta^2)^{1/2}z}\, d\alpha\, d\beta, \qquad j=\sqrt{-1} \quad (5)$$

where α and β are the separation constants which are continuous eigenvalues for this case. At $z = 0$

$$\left.\frac{\partial\varphi}{\partial z}\right|_{z=0} = \frac{x P_y}{4\pi(x^2+y^2+d^2)^{3/2}} = \int_{-\infty}^{\infty}\int_{-\infty}^{\infty} F(\alpha,\beta)e^{j2\pi\alpha x}\, e^{j2\pi\beta y}\, d\alpha\, d\beta \quad (6)$$

where

$$F(\alpha,\beta) = -2\pi(\alpha^2+\beta^2)^{1/2}\, G(\alpha,\beta).$$

Using Fourier integral transforms [13]-[14] it can be shown that

$$F(\alpha,\beta) = -\frac{j P_y \alpha e^{-2\pi d(\alpha^2+\beta^2)^{1/2}}}{2(\alpha^2+\beta^2)^{1/2}}. \quad (7)$$

Therefore,

$$\varphi = \int_{-\infty}^{\infty}\int_{-\infty}^{\infty} \cdot\frac{j P_y \alpha e^{-2\pi(\alpha^2+\beta^2)^{1/2}(d+z)}\, e^{j2\pi\alpha x}\, e^{j2\pi\beta y}\, d\alpha\, d\beta}{4\pi(\alpha^2+\beta^2)}. \quad (8)$$

If we let $\alpha = \rho\cos\theta$, $\beta = \rho\sin\theta$, and $\rho^2 = \alpha^2+\beta^2$, then

$$\varphi = \frac{j P_y}{4\pi}\int_0^{\infty}\int_0^{2\pi} \cos\theta\, e^{-2\pi\rho(d+z)} \cdot e^{j2\pi\rho(x\cos\theta + y\sin\theta)}\, d\theta\, d\rho. \quad (9)$$

After integration with respect to ρ followed by the substitution $s = e^{j\theta}$

$$\varphi = -\frac{j P_y}{8\pi^2}\oint_C \frac{(S^2+1)\, dS}{S[S^2(y+jx) - 2(d+z)S - (y-jx)]} \quad (10)$$

where C is circle of unit radius in the complex plane, and this can be evaluated by the method or residues to give

$$\varphi = \frac{x P_y}{4\pi(x^2+y^2)}\left\{\frac{d+z}{[x^2+y^2+(d+z)^2]^{1/2}} - 1\right\}. \quad (11)$$

Using equation (2) with equation (11) yields

$$H_x = \frac{P_y}{4\pi}\left\{\frac{(y^2-x^2)[x^2+y^2+(d+z)^2]^{3/2} - (d+z)\{(y^2-x^2)[y^2+(d+z)^2] - 2x^4\}}{(x^2+y^2)^2[x^2+y^2+(d+z)^2]^{3/2}}\right\}$$

$$H_y = \frac{xyP_y}{4\pi}\left\{\frac{(d+z)[3x^2+3y^2+2(d+z)^2] - 2[x^2+y^2+(d+z)^2]^{3/2}}{(x^2+y^2)^2[x^2+y^2+(d+z)^2]^{3/2}}\right\}$$

$$H_z = -\frac{x P_y}{4\pi[x^2+y^2+(d+z)^2]^{3/2}}. \quad (12)$$

Subtracting $\bar{H}_d$ as calculated by equation (1) from $\bar{H}$ yields the following expressions for $\bar{H}_v$:

$$H_{xv} = \frac{P_y}{4\pi(x^2+y^2)^2[x^2+y^2+(d+z)^2]^{3/2}} \times\{(y^2-x^2)[x^2+y^2+(d+z)^2]^{3/2} + (d+z)[(x^2-y^2)(d+z)^2 - 2y^4 - x^2y^2 + x^4]\},$$

$$H_{yv} = H_y, \qquad H_{zv} = 0. \quad (13)$$

Some representative plots of $\bar{H}$ and $\bar{H}_v$ are presented in Fig. 1.

For points on the z axis, equations (12) become, on the application of L'Hopital's rule,

$$H_x = \frac{P_y}{8\pi(d+z)^2}, \qquad H_y = H_z = 0. \quad (14)$$

Since $H_{yd} = 0$ and $H_{zv} = 0$, the ratios of the components of $\bar{H}_d$ and $\bar{H}$ are

$$\frac{H_{xd}}{H_x} = \frac{(d+z)(x^2+y^2)^2}{(y^2-x^2)[x^2+y^2+(d+z)^2]^{3/2} - (d+z)\{(y^2-x^2)[y^2+(d+z)^2] - 2x^4\}}, \quad \frac{H_{yd}}{H_y} = 0, \quad \frac{H_{zd}}{H_z} = 1. \quad (15)$$

On the z axis, $H_{xd}/H_x = 2$, which indicates that H_{xv} is the direction opposite to H_{xd} and one-half its magnitude. By setting $H_{xd}/H_x = \infty$ and $y = z = 0$, the value of x on the x axis for which $H_x = 0$ can be found to be

$$x = \pm d\left(\frac{1+\sqrt{5}}{2}\right)^{1/2}. \quad (16)$$

Sphere

Grynszpan [15] has calculated the magnetic field produced by a current dipole located in a sphere. This result will be outlined here. Since a radially oriented dipole produces $\bar{H} = 0$ outside of the sphere because of the symmetry conditions, only a tangential dipole need be considered. Without loss of generality the tangential dipole is assumed to be pointing in the positive x-direction and located at $r = a$, $\theta = 0°$, and $\varphi = 0°$, as shown in Fig. 2A. The magnetic field produced by this dipole is calculated through the use of the vector magnetic potential, $\bar{A}$, from which $\bar{H}$ can be calculated by

$$\bar{H} \equiv \frac{\nabla\times\bar{A}}{\mu}. \quad (17)$$

The following expression for $\bar{A}$ has been developed by Geselowitz [12]:

$$\bar{A} = \frac{1}{4\pi}\iiint\frac{\mu\bar{J}^i}{R}\, dv - \frac{\mu\sigma}{4\pi}\oiint\frac{V}{R}\,\overline{ds} \quad (18)$$

where the terms are as defined previously. In a manner similar

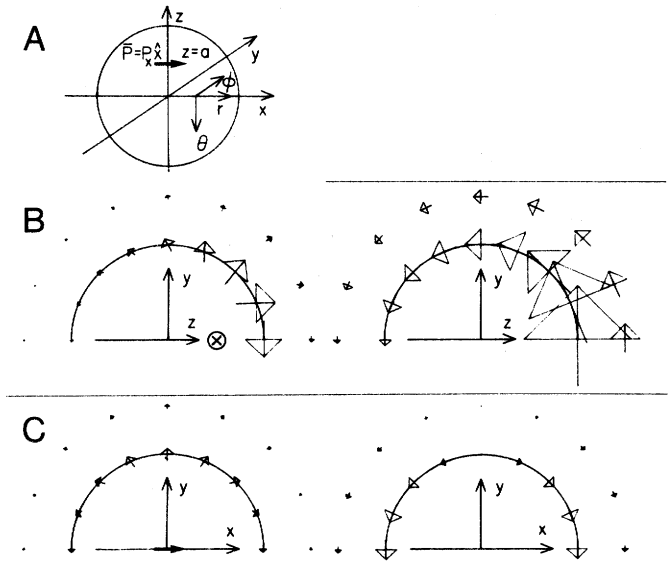

Fig. 2. Magnetic fields of a dipole in a sphere. For the field plots, "a" is equal to one-half the radius of the sphere. The scale for the arrows is arbitrary but consistent for all plots in this figure. ⊗ indicates the dipole going into the page. Note that the dipole location is not indicated on the plots of $\bar{H}_v$ (those on the right side of the figure); it would be same as in the corresponding plot of $\bar{H}$. The fields are plotted in the following planes: (B) $x = 0$; and (C) $z = 0$ (the solid arrow represents the projection of the current dipole on this plane).

to that of equation (4), the term containing the volume integral represents the vector magnetic potential due to the dipole alone, while the other term represents the potential due to the current flowing in the volume conductor. In spherical coordinates

$$\frac{1}{R} = \frac{1}{r'} \sum_{n=0}^{\infty} \sum_{m=0}^{n} \left(\frac{r}{r'}\right)^n (2 - \delta_m^\circ) \frac{(n-m)!}{(n+m)!} \times \cos m(\varphi' - \varphi) P_n^m(\cos\theta) P_n^m(\cos\theta') \tag{19}$$

where

$$\delta_m^\circ = 1, \quad m = 0$$
$$= 0 \quad m \neq 0,$$

P_n^m is an associated Legendre polynomial, and the primed variables refer to the field point, while the unprimed variables refer to an element of volume or surface. In equation (18) the electric potential, V, on the surface is given by

$$V = \frac{P_x \cos\varphi}{4\pi\sigma R_s^2} \sum_{l=1}^{\infty} \frac{(2l+1) f^{l-1}}{l} P_l'(\cos\theta) \tag{20}$$

where R_s is the radius of the sphere and $f = a/R_s$. Performing the indicated integrations over the surface of the sphere and using the orthogonality properties of Legendre polynomials and trigonometric functions allows the evaluation of the integral. Applying equation (17) to the evaluated integral, using some known relationships for infinite series of Legendre polynomials, and dropping the primes on the field point variables as no confusion will result yields

$$H_{\theta v} = \frac{\sin\varphi P_x}{4\pi r^2 \gamma^{1/2}} \left[\frac{\cos\theta}{\sin^2\theta} \left(\cos\theta - \frac{r}{a} + \frac{r\gamma^{1/2}}{a} \right) + 1 \right]$$

$$H_{\varphi v} = \frac{\cos\varphi P_x}{4\pi r^2 \gamma^{3/2}} \left[\cos\theta - \frac{a}{r} - \frac{\gamma}{\sin^2\theta} \left(\cos\theta - \frac{r}{a} + \frac{r\gamma^{1/2}}{a} \right) \right]$$

$$\gamma = \left[1 - \frac{2a\cos\theta}{r} + \left(\frac{a}{r}\right)^2 \right]. \tag{21}$$

The field of the dipole alone can be calculated by dealing with the volume integral of equation (18), or, as is done in the paper, by using equation (1) directly. Adding $\bar{H}_d$ to $\bar{H}_v$ yields

$$H_r = \frac{a \sin\theta \sin\varphi P_x}{4\pi r^2 \gamma^{3/2}}$$

$$H_\theta = \frac{\sin\varphi P_x}{4\pi r^2 \gamma^{3/2}} \left[\frac{\gamma\cos\theta}{\sin^2\theta} \left(\cos\theta - \frac{r}{a} + \frac{r\gamma^{1/2}}{a} \right) - \frac{a}{r} \left(\cos\theta - \frac{a}{r} \right) \right]$$

$$H_\varphi = \frac{\cos\varphi P_x}{4\pi r^2 \gamma^{1/2} \sin^2\theta} \left[\frac{r}{a} - \cos\theta - \frac{r\gamma^{1/2}}{a} \right]. \tag{22}$$

In Fig. 2 are presented some plots of $\bar{H}$ and $\bar{H}_v$ produced by a dipole in a sphere as calculated using equations (21) and (22).

Since equations (21) show that $H_{rv} = 0$, the ratios of the components of $\bar{H}_d$ and $\bar{H}$ are

$$\frac{H_{\theta d}}{H_\theta} = \frac{\frac{a\cos\theta}{r} - 1}{\frac{\gamma\cos\theta}{\sin^2\theta} \left(\cos\theta - \frac{r}{a} + \frac{r}{a}\gamma^{1/2} \right) - \frac{a}{r} \left(\cos\theta - \frac{a}{r} \right)}$$

$$\frac{H_{\varphi d}}{H_\varphi} = \frac{\frac{\sin^2\theta}{\gamma} \left(\cos\theta - \frac{a}{r} \right)}{\cos\theta - \frac{r}{a} + \frac{r}{a}\gamma^{1/2}} \frac{H_{rd}}{H_r} = 1. \tag{23}$$

On the z axis

$$\frac{H_{\varphi d}}{H_\varphi} = \frac{2\left(K\frac{r}{a} - 1\right)}{1 - K\frac{a}{r}} \tag{24}$$

where

$$K = 1, \quad z > R_s$$
$$K = -1, \quad z < R_s.$$

Prolate Spheroid

For the prolate spheroid shown in Fig. 3A, $\bar{H}$ outside the spheroid produced by the current dipole moments P_{ξ_0}, P_{η_0}, and P_{φ_0} is calculated using equation (4). The calculation of the volume integral which gives $\bar{H}_d$ is straightforward since $\bar{J}^i\, dv$ becomes the current dipole moment $\bar{P}$, and it can be expressed exactly in rectangular coordinates which are related to the prolate spheroidal coordinates as follows:

$$x = C[(1 - \xi^2)(\eta^2 - 1)]^{1/2} \sin\varphi$$
$$y = C[(1 - \xi^2)(\eta^2 - 1)]^{1/2} \cos\varphi$$
$$z = C\xi\eta \tag{25}$$

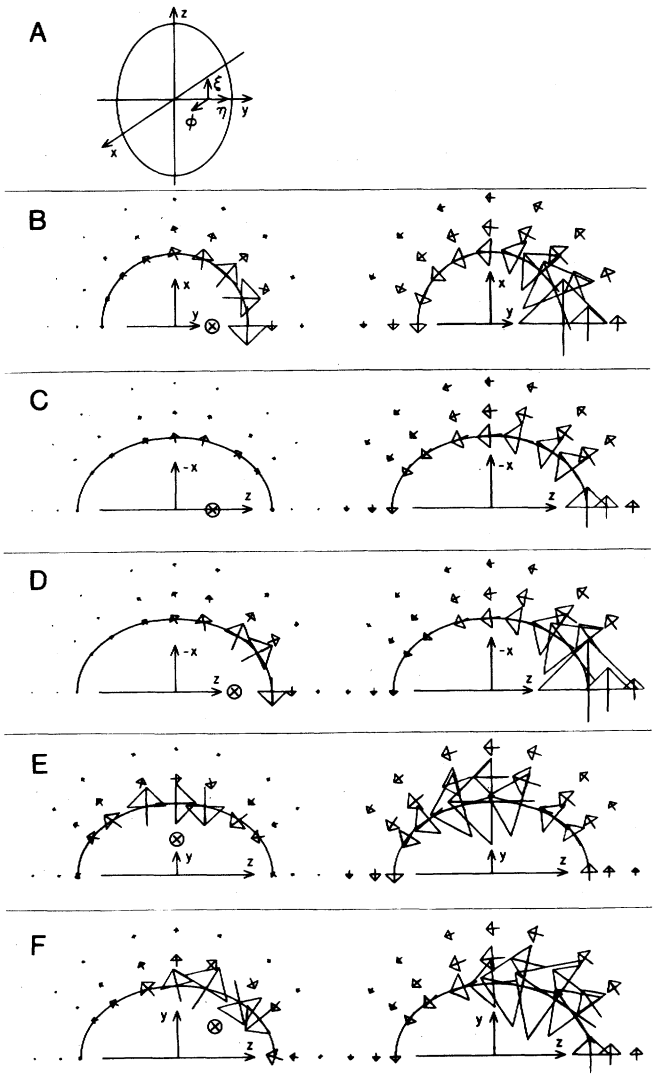

Fig. 3. Magnetic fields of dipoles in a prolate spheroid. For the spheroid shown, $C = 1.0$ and $\eta_a = 1.5$. The scale is arbitrary but consistent for all plots in this figure. Dipole locations (with $\varphi_0 = 0$ for all cases) and the planes in which the fields are plotted are as follows: (B) $\xi_0 = 0.0$, $\eta_0 = 1.15$, $z = 0$; (C) $\xi_0 = 0.575$, $\eta_0 = 1.0$, $y = 0$; (D) $\xi_0 = 0.95$, $\eta_0 = 1.0$, $y = 0$; (E) $\xi_0 = 0.0$, $\eta_0 = 1.15$, $x = 0$; and (F) $\xi_0 = 0.5$, $\eta_0 = 1.15$, $x = 0$.

where the prolate spheroidal variables are in the ranges $-1 \leqslant \xi \leqslant 1$, $1 \leqslant \eta$, $0 \leqslant \varphi < 2\pi$ and C is a constant. Therefore, $\bar{H}_d$ can be calculated using equation (1).

The evaluation of the surface integral in equation (4), which gives $\bar{H}_v$, requires an expression for the electric potential, V, produced on the surface of the spheroid (with $\eta = \eta_a$) by the various current dipoles. This expression can be adapted from Berry [16] as

$$V = \frac{1}{4\pi\sigma C^2} \sum_{l=0}^{\infty} \sum_{k=0}^{l} \frac{(2 - \delta_k^0)(2l+1)(l-k)!\, P_l^k(\xi)}{(\eta_a^2 - 1)(l+k)!\, P_l^{k\circledcirc}(\eta_a)} \times \left[\frac{P_{\xi_0} P_l^k(\eta_0) P_l^{k\circledcirc}(\xi_0) \cos k(\varphi - \varphi_0)}{h_{\xi_0}} + \frac{P_{\eta_0} P_l^{k\circledcirc}(\eta_0) P_l^k(\xi_0) \cos k(\varphi - \varphi_0)}{h_{\eta_0}} + \frac{P_{\varphi_0} P_l^k(\eta_0) P_l^k(\xi_0)\, k \sin k(\varphi - \varphi_0)}{h_{\varphi_0}} \right] \tag{26}$$

where ξ_0, η_0, and φ_0 refer to the location of the dipole, while ξ, η_a, and φ refer to locations on the surface of the spheroid and

$$P_l^{k\circledcirc}(\xi_0) = \frac{\partial P_l^k(\xi_0)}{\partial \xi_0}.$$

The metric coefficients are

$$h_\xi = C\left(\frac{\eta^2 - \xi^2}{1 - \xi^2}\right)^{1/2}$$

$$h_\eta = C\left(\frac{\eta^2 - \xi^2}{\eta^2 - 1}\right)^{1/2}$$

$$h_\varphi = C[(1 - \xi^2)(\eta^2 - 1)]^{1/2} \tag{27}$$

with $\xi = \xi_0$, $\eta = \eta_0$, and $\varphi = \varphi_0$. The following infinite series expansion for the $1/R$ term which appears in the surface integral can be obtained from Smythe: [17]

$$\frac{1}{R} = \frac{1}{C} \sum_{n=0}^{\infty} \sum_{m=0}^{n} (\partial - \delta_m^0)(-1)^m (2n+1) \left[\frac{(n-m)!}{(n+m)!}\right]^2 \times P_n^m(\xi') P_n^m(\xi) Q_n^m(\eta') P_n^m(\eta_a) \cos m(\varphi' - \varphi) \tag{28}$$

where again the primed variables apply to the field point and the unprimed apply to an element of surface. Equations (26), (27), and (28) can be substituted into the surface integral of equation (4). In order to simplify the indicated integrations, the vector integrand is expressed in rectangular components and $\varphi_0 = 0$ is assumed. For a P_{ξ_0} dipole the integral becomes

$$\oiint V \nabla \frac{1}{R} \times d\bar{s} = \frac{P_{\xi_0}}{4\pi\sigma C^2 h_{\xi_0}} \int_0^{2\pi} \int_{-1}^{1} \cdot \left[\sum_{l=0}^{\infty} \sum_{k=0}^{l} \frac{(2 - \delta_k^0)(2l+1)(l-k)!\, P_l^k(\xi)}{(\eta_a^2 - 1)(l+k)!\, P_l^{k\circledcirc}(\eta_a)} \times P_l^k(\eta_0) P_l^{k\circledcirc}(\xi_0) \cos k\varphi \right] \times \left\{ \sum_{n=0}^{\infty} \sum_{m=0}^{n} (2 - \delta_m^0)(-1)^m (2n+1) \times \left[\frac{(n-m)!}{(n+m)!}\right]^2 P_n^m(\xi') Q_n^m(\eta') P_n^m(\eta_a) \times (\eta_a^2 - 1)^{1/2} \times \left[\left(\frac{-m \sin m(\varphi' - \varphi) \xi \sin \varphi P_n^m(\xi)}{(1 - \xi^2)^{1/2}} - (1 - \xi^2)^{1/2} \cos \varphi P_n^{m\circledcirc}(\xi) \cos m(\varphi' - \varphi) \right) \hat{x} + \left(\frac{-m \sin m(\varphi' - \varphi) \xi \cos \varphi P_n^m(\xi)}{(1 - \xi^2)^{1/2}} + (1 - \xi^2)^{1/2} \sin \varphi P_n^{m\circledcirc}(\xi) \cos m(\varphi' - \varphi) \right) \hat{y} + \left(\frac{\eta_a m \sin m(\varphi' - \varphi) P_n^m(\xi)}{(\eta_a^2 - 1)^{1/2}} \right) \hat{z} \right] \right\} d\xi\, d\varphi \tag{29}$$

where $\hat{x}$, $\hat{y}$, and $\hat{z}$ are rectangular unit vectors.

In order to evaluate equation (29), use is made of the orthogonality relationships between trigonometric functions. These require $k = m \pm 1$ for the $\hat{x}$ and $\hat{y}$ components with $m > 0$ except for the second term of the $\hat{x}$ component where $m \geq 0$. For the $\hat{z}$ component, the orthogonality relationships require $k = m$ with $m > 0$. For all other combinations of k and m, integration with respect to φ is equal to zero. Imposing these limitations on k and m in the integration with respect to ξ, the following relationships can be developed. Considering only the functions of ξ in the $\hat{x}$ component of equation (29) and with $k = m - 1$, integration with respect to ξ gives

$$\int_{-1}^{1} P_l^{m-1}(\xi)\left[\frac{m\xi P_n^m(\xi)}{(1-\xi^2)^{1/2}} - (1-\xi^2)^{1/2} P_n^{m\,@}(\xi)\right] d\xi$$

$$= \frac{2(n+m)!}{(2n+1)(n-m)!}, \quad l = n$$

$$= 0, \quad l \neq n. \tag{30}$$

For $k = m + 1$, integration with respect to ξ gives

$$\int_{-1}^{1} P_l^{m+1}(\xi)\left[\frac{m\xi P_n^m(\xi)}{(1-\xi^2)^{1/2}} + (1-\xi^2)^{1/2} P_n^{m\,@}(\xi)\right] d\xi$$

$$= \frac{2(n+m+1)!}{(2n+1)(n-m-1)!}, \quad l = n$$

$$= 0, \quad l \neq n. \tag{31}$$

With appropriate change in sign, these same relations also apply to the $\hat{y}$ component in equation (29). For the $\hat{z}$ component, considering only the functions of ξ with $k = m$, integration with respect to ξ gives

$$\int_{-1}^{1} P_l^m(\xi) P_n^m(\xi) d\xi = \frac{2(n+m)!}{(2n+1)(n-m)!}, \quad l = n$$

$$= 0, \quad l \neq n. \tag{32}$$

Using these relationships and recognizing the special case in the $\hat{x}$ component when $m = 0$, the integral in equation (29) can be evaluated to give the following where the primes on the field point coordinates have been dropped:

$$H_{xv} = \frac{P_{\xi_0}(1-\xi_0)^{1/2}}{4\pi C^2(\eta_a^2-1)^{1/2}(\eta_0^2-\xi_0^2)^{1/2}}$$

$$\times \left\{ \sum_{n=1}^{\infty} \sum_{m=1}^{n} (2n+1)(-1)^m \left[\frac{(n-m)!}{(n+m)!}\right]^2 \right.$$

$$\times \cos m\varphi P_n^m(\xi) Q_n^m(\eta) P_n^m(\eta_a)$$

$$\times \left[\frac{(n+m)(n-m+1)P_n^{m-1}(\eta_0)P_n^{m-1\,@}(\xi_0)}{P_n^{m-1\,@}(\eta_a)}\right.$$

$$\left. - \frac{P_n^{m+1}(\eta_0)P_n^{m+1\,@}(\xi_0)}{P_n^{m+1\,@}(\eta_a)}\right]$$

$$\left. - \sum_{n=1}^{\infty} \frac{(2n+1)P_n^1(\eta_0)P_n^{1\,@}(\xi_0)P_n(\xi)Q_n(\eta)P_n(\eta_a)}{P_n^{1\,@}(\eta_a)}\right\}$$

$$H_{yv} = \frac{P_{\xi_0}(1-\xi_0^2)^{1/2}}{4\pi C^2(\eta_a^2-1)^{1/2}(\eta_0^2-\xi_0^2)^{1/2}}$$

$$\times \left| \sum_{n=1}^{\infty} \sum_{m=1}^{n} (2n+1)(-1)^m \left[\frac{(n-m)!}{(n+m)!}\right]^2 \right.$$

$$\times \sin m\varphi P_n^m(\xi) Q_n^m(\eta) P_n^m(\eta_a)$$

$$\times \left[-\frac{(n+m)(n-m+1)P_n^{m-1}(\eta_0)P_n^{m-1\,@}(\xi_0)}{P_n^{m-1\,@}(\eta_a)}\right.$$

$$\left. - \frac{P_n^{m+1}(\eta_0)P_n^{m+1\,@}(\xi_0)}{P_n^{m+1\,@}(\eta_a)}\right]$$

$$H_{zv} = \frac{\eta_a P_{\xi_0}(1-\xi_0^2)^{1/2}}{2\pi C^2(\eta_a^2-1)(\eta_0^2-\xi_0^2)^{1/2}} \sum_{n=1}^{\infty} \sum_{m=1}^{n} \frac{(2n+1)(-1)^m}{P_n^{m\,@}(\eta_a)}$$

$$\times m \sin m\varphi \left[\frac{(n-m)!}{(n+m)!}\right]^2$$

$$\times P_n^m(\eta_0)P_n^{m\,@}(\xi_0)P_n^m(\xi)Q_n^m(\eta)P_n^m(\eta_a). \tag{33}$$

For a P_{η_0} dipole, the solution is the same as for the P_{ξ_0} dipole, except that the following substitutions must be made in equations (33):

$$(1-\xi_0^2)^{1/2} = (\eta_0^2-1)^{1/2}$$

$$P_n^{m\,@}(\xi_0) = P_n^m(\xi_0)$$

$$P_n^m(\eta_0) = P_n^{m\,@}(\eta_0). \tag{34}$$

The solution for a P_{φ_0} dipole proceeds along the same lines and gives

$$H_{xv} = \frac{P_{\varphi_0}}{4\pi C^2(\eta_0^2-1)^{1/2}(1-\xi_0^2)^{1/2}(\eta_a^2-1)^{1/2}}$$

$$\times \sum_{n=1}^{\infty} \sum_{m=1}^{n} (2n+1)(-1)^m$$

$$\times \left[\frac{(n-m)!}{(n+m)!}\right]^2 \sin m\varphi P_n^m(\xi) Q_n^m(\eta) P_n^m(\eta_a)$$

$$\times \left[\frac{(m-1)(n+m)(n-m+1)P_n^{m-1}(\eta_0)P_n^{m-1}(\xi_0)}{P_n^{m-1\,@}(\eta_a)}\right.$$

$$\left. - \frac{(m+1)P_n^{m+1}(\eta_0)P_n^{m+1}(\xi_0)}{P_n^{m+1\,@}(\eta_a)}\right]$$

$$H_{yv} = \frac{P_{\varphi_0}}{4\pi C^2(\eta_0^2-1)^{1/2}(1-\xi_0^2)^{1/2}(\eta_a^2-1)^{1/2}}$$

$$\times \left\{ \sum_{n=1}^{\infty} \sum_{m=1}^{n} (2n+1)(-1)^m \right.$$

$$\times \left[\frac{(n-m)!}{(n+m)!}\right]^2 \cos m\varphi P_n^m(\xi) Q_n^m(\eta) P_n^m(\eta_a)$$

$$\times \left[\frac{(m-1)(n+m)(n-m+1)P_n^{m-1}(\eta_0)P_n^{m-1}(\xi_0)}{P_n^{m-1\,@}(\eta_a)}\right.$$

$$\left. + \frac{(m+1)P_n^{m+1}(\eta_0)P_n^{m+1}(\xi_0)}{P_n^{m+1\,@}(\eta_a)}\right]$$

$$\left. + \sum_{n=1}^{\infty} \frac{(2n+1)P_n^1(\eta_0)P_n^1(\xi_0)P_n(\xi)Q_n(\eta)P_n(\eta_a)}{P_n^{1\,@}(\eta_a)}\right\}$$

$$H_{zv} = -\frac{\eta_a P_{\varphi_0}}{2\pi C^2(\eta_a^2 - 1)(\eta_0^2 - 1)^{1/2}(1 - \xi_0^2)^{1/2}} \times \sum_{n=1}^{\infty}\sum_{m=1}^{n} \frac{(2n+1)(-1)^m}{P_n^{m\circledcirc}(\eta_a)} \times \left[\frac{(n-m)!}{(n+m)!}\right]^2 m^2 \times \cos m\varphi P_n^m(\eta_0)P_n^m(\xi_0)P_n^m(\xi)Q_n^m(\eta)P_n^m(\eta_a). \quad (35)$$

Equations (33), (34), and (35) provide means for calculating $\bar{H}_v$ produced by the volume currents flowing in the spheroid which are generated by P_{ξ_0}, P_{η_0}, and P_{φ_0} current dipoles, respectively. In order to obtain $\bar{H}$, $\bar{H}_d$ as calculated from equation (1) must be added to these expressions. Some representative plots of $\bar{H}$ and $\bar{H}_v$ produced by various dipoles in a prolate spheroid are presented in Fig. 3. If $\xi_0 = 1$ or $\eta_0 = 1$, then the following relations must be used in order to perform the calculations:

$$(1 - \xi_0^2)^{1/2}P_n^{m\circledcirc}(\xi_0) = \frac{-n(n+1)}{2}, \quad m = 1$$
$$= 0, \quad m \neq 1$$
$$(\eta_0^2 - 1)^{1/2}P_n^{m\circledcirc}(\eta_0) = \frac{n(n+1)}{2}, \quad m = 1$$
$$= 0, \quad m \neq 1. \quad (36)$$

For the plots in Fig. 3, the infinite series in the expressions for $\bar{H}_v$ are truncated for n greater than 10. The values of the associated Legendre polynomials are calculated using the recurrence relationships and are in agreement with values available in standard tables [18]. Several tests of the ability of this number of terms to accurately represent the solution were performed. One test involves calculating the field for a dipole located at various points on the axis and pointing in the $\hat{z}$ direction. Because of the symmetry present for these conditions, the $\bar{H}$ should be equal to zero; therefore, $\bar{H}_d = -\bar{H}_v$. For this test, $\bar{H}_v$ is equal and opposite to $\bar{H}_d$ to within 0.2% in the worst case for the points at which the field is calculated. Another test was performed by varying the maximum value of n for a P_{ξ_0} dipole located off the z axis ($\xi_0 = 0$, $\eta_0 = 1.15$). As expected, the differences between the series solutions decrease as the maximum value of n increases. For this test, the maximum difference between the solution for $n = 9$ and $n = 10$ is approximately 8%. These comparisons are made for the field in the plane normal to the dipole and interestingly the greatest difference occurs at the point which is farthest from the dipole, which is where $\bar{H}$ is smallest. Since the expressions for $\bar{H}_v$ are infinite series, no convenient expression for the ratios of the components of $\bar{H}_d$ and $\bar{H}$ can be developed. These ratios can be calculated for particular locations as required. As an example, these ratios for the normal and tangential components of the fields on the surface of the spheroid of Fig. 3F are presented in Table 1.

TABLE I
COMPARISON OF $\bar{H}_d/\bar{H}$ RATIOS FOR NORMAL AND TANGENTIAL FIELD COMPONENTS ON THE SURFACE OF A PROLATE SPHEROID

Field location	H_η (normal)	$H_{d\eta}/H_\eta$	H_ξ (tangential)	$H_{d\xi}/H_\xi$
1	0.05	1.00	-0.07	-3.15
2	0.11	1.62	-0.11	-2.07
3	0.18	1.50	-0.15	-1.85
4	0.42	1.27	-0.24	-2.00
5	0.84	1.12	-0.20	-5.10
6	1.21	1.03	0.44	5.97
7	-0.83	1.12	0.83	4.02
8	-0.93	1.13	-0.01	-242.71
9	-0.43	1.0	-0.14	-5.75

Note: Ratios are calculated for the fields produced by the dipole as shown in Fig. 3F. Field locations are on the surface of the spheroid with location 1 on negative z axis, location 5 on the positive y axis, and location 9 on the positive z axis. Note that for the $x = 0$ plane in Fig. 3F, $H_\varphi = H_{\varphi v} = H_{\varphi d} = 0$.

Oblate Spheroid

For the oblate spheroid the development proceeds in the same manner as for the prolate spheroid. In the oblate spheroidal coordinate system presented in Fig. 4A

$$x = C\xi\zeta$$
$$y = C[(1 - \xi^2)(1 + \zeta^2)]^{1/2}\cos\varphi$$
$$z = C[(1 - \xi^2)(1 + \zeta^2)]^{1/2}\sin\varphi \quad (37)$$

where $-1 \leqslant \xi \leqslant 1$; $0 \leqslant \zeta$; $0 \leqslant \varphi < 2\pi$, and C is a constant. The metric coefficients are

$$h_\xi = C\left(\frac{\xi^2 + \zeta^2}{1 - \xi^2}\right)^{1/2}$$
$$h_\zeta = C\left(\frac{\xi^2 + \zeta^2}{1 + \zeta^2}\right)^{1/2}$$
$$h_\varphi = C[(1 - \xi^2)(1 + \zeta^2)]^{1/2}. \quad (38)$$

Again $\bar{H}_d$ can be calculated using equation (1), the expression for the electrical potential produced on the surface of the oblate spheroid (with $\zeta = \zeta_a$) can be adapted from Berry [16], and $1/R$ in oblate spheroid coordinates can be expressed as an infinite series [19]. Proceeding with the same general methods as those used for the prolate spheroid, expressions for $\bar{H}_v$ for the oblate spheroid can be developed. In the following expressions, ξ_0 and ζ_0 refer to the location of the dipole (with $\varphi_0 = 0$), while ξ, ζ, and φ refer to the field point. For a P_{ξ_0} dipole, the following expression for $\bar{H}_v$ is developed:

$$H_{xv} = \frac{\zeta_a P_{\xi_0}(1 - \xi_0^2)^{1/2}}{8\pi C^2(1 + \zeta_a^2)(\xi_0^2 + \zeta_0^2)^{1/2}} \times \sum_{n=1}^{\infty}\sum_{m=1}^{n} \frac{j(2n+1)(-1)^m}{P_n^{m\circledcirc}(j\zeta_a)}\left[\frac{(n-m)!}{(n+m)!}\right]^2 \times m \sin m\varphi P_n^m(j\zeta_a)Q_n^m(j\zeta)P_n^m(\xi)P_n^m(j\zeta_0)P_n^{m\circledcirc}(\xi_0)$$

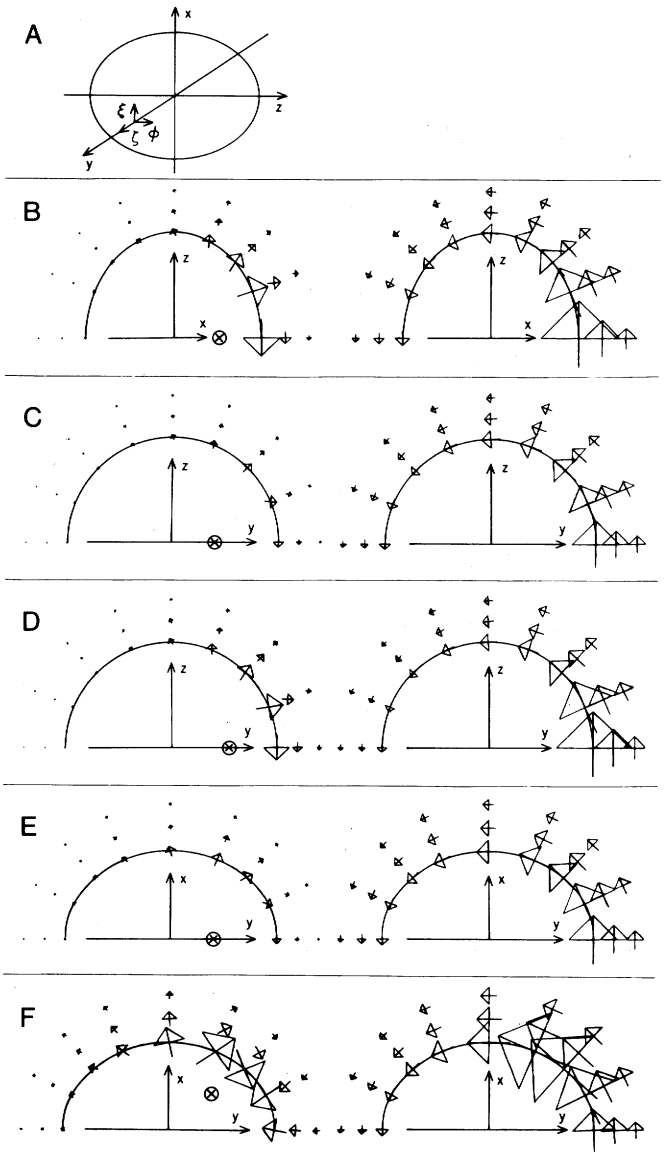

Fig. 4. Magnetic fields of dipoles in an oblate spheroid. For the spheroid shown, $C = 1.0$ and $\zeta_a = 1.5$. The scale is arbitrary but consistent for all plots in this figure. Dipole locations (with $\varphi_0 = 0$ for all cases) and the planes on which the fields are plotted are as follows: (B) $\xi_0 = 1.0$, $\zeta_0 = 0.75$, $y = 0$; (C) $\xi_0 = 0.66$, $\zeta_0 = 0.0$, $x = 0$; (D) $\xi_0 = 0.05$, $\zeta_0 = 0.0$, $x = 0$; (E) $\xi_0 = 0.66$, $\zeta_0 = 0.0$, $z = 0$; (F) $\xi_0 = 0.8$, $\zeta_0 = 0.75$, $z = 0$.

$$H_{yv} = \frac{P_{\xi_0}(1-\xi_0^2)^{1/2}}{4\pi C^2(1+\zeta_a^2)^{1/2}(\xi_0^2+\zeta_0^2)^{1/2}} \times \sum_{n=1}^{\infty}\sum_{m=1}^{n} j(2n+1)(-1)^m \times \left[\frac{(n-m)!}{(n+m)!}\right]^2 P_n^m(j\zeta_a)Q_n^m(j\zeta)P_n^m(\xi)\sin m\varphi \times \left[\frac{-(n+m)(n-m+1)P_n^{m-1}(j\zeta_0)P_n^{m-1\circledcirc}(\xi_0)}{P_n^{m-1\circledcirc}(j\zeta_a)} - \frac{P_n^{m+1}(j\zeta_0)P_n^{m+1\circledcirc}(\xi_0)}{P_n^{m+1\circledcirc}(j\zeta_a)}\right]$$

$$H_{zv} = \frac{P_{\xi_0}(1-\xi_0^2)^{1/2}}{4\pi C^2(1+\zeta_a^2)^{1/2}(\xi_0^2+\zeta_0^2)^{1/2}} \times \left\{\sum_{n=1}^{\infty}\sum_{m=1}^{n} j(2n+1)(-1)^m \times \left[\frac{(n-m)!}{(n+m)!}\right]^2 P_n^m(j\zeta_a)Q_n^m(j\zeta)P_n^m(\xi)\cos m\varphi \times \left[\frac{(n+m)(n-m+1)P_n^{m-1}(j\zeta_0)P_n^{m-1\circledcirc}(\xi_0)}{P_n^{m-1\circledcirc}(j\zeta_a)} - \frac{P_n^{m+1}(j\zeta_0)P_n^{m+1\circledcirc}(\xi_0)}{P_n^{m+1\circledcirc}(j\zeta_a)}\right] - \sum_{n=1}^{\infty}\frac{j(2n+1)P_n^1(j\zeta_0)P_n^{1\circledcirc}(\xi_0)P_n(j\zeta_a)Q_n(j\zeta)P_n(\xi)}{P_n^{1\circledcirc}(j\zeta_a)}\right\}. \quad (39)$$

For a P_{ζ_0} dipole, equation (39) can be used after the following substitutions are made:

$$(1-\xi_0^2)^{1/2} = (1+\zeta_0^2)^{1/2}$$
$$P_n^m(j\zeta_0) = P_n^{m\circledcirc}(j\zeta_0)$$
$$P_n^{m\circledcirc}(\xi_0) = P_n^m(\xi_0). \quad (40)$$

For a P_{φ_0} dipole, the expression is

$$H_{xv} = -\frac{\zeta_a P_{\varphi_0}}{2\pi C^2(1+\zeta_a^2)(1+\zeta_0^2)^{1/2}(1-\xi_0^2)^{1/2}} \times \sum_{n=1}^{\infty}\sum_{m=1}^{n}\frac{j(2n+1)(-1)^m}{P_n^{m\circledcirc}(j\zeta_a)} \times \left[\frac{(n-m)!}{(n+m)!}\right]^2 m^2 \times \cos m\varphi P_n^m(j\zeta_0)P_n^m(\xi_0)P_n^m(\xi)Q_n^m(j\zeta)P_n^m(j\zeta_a)$$

$$H_{yv} = \frac{P_{\varphi_0}}{4\pi C^2(1+\zeta_a^2)^{1/2}(1+\zeta_0^2)^{1/2}(1-\xi_0^2)^{1/2}} \times \left\{\sum_{n=1}^{\infty}\sum_{m=1}^{n} j(2n+1)(-1)^m \cos m\varphi \times P_n^m(\xi)Q_n^m(j\zeta)P_n^m(j\zeta_a) \times \left[\frac{(m-1)(n+m)(n-m+1)P_n^{m-1}(j\zeta_0)P_n^{m-1}(\xi_0)}{P_n^{m-1\circledcirc}(j\zeta_a)} + \frac{(m+1)P_n^{m+1}(j\zeta_0)P_n^{m+1}(\xi_0)}{P_n^{m+1\circledcirc}(j\zeta_a)}\right] + \sum_{n=1}^{\infty}\frac{j(2n+1)P_n^1(j\zeta_0)P_n^1(\xi_0)P_n(\xi)Q_n(j\zeta)P_n(j\zeta_a)}{P_n^{1\circledcirc}(j\zeta_a)}\right\}$$

$$H_{zv} = \frac{P_{\varphi_0}}{4\pi C^2(1+\zeta_a^2)^{1/2}(1+\zeta_0^2)^{1/2}(1-\xi_0^2)^{1/2}} \times \left\{ \sum_{n=1}^{\infty} \sum_{m=1}^{n} j(2n+1)(-1)^m \times \sin m\varphi P_n^m(\xi) Q_n^m(j\zeta) P_n^m(j\zeta_a) \left[\frac{(n-m)!}{(n+m)!}\right]^2 \times \left[\frac{(m-1)(n+m)(n-m+1)P_n^{m-1}(j\zeta_0)P_n^{m-1}(\xi_0)}{P_n^{m-1^{\circledcirc}}(j\zeta_a)} - \frac{(m+1)P_n^{m+1}(j\zeta_0)P_n^{m+1}(\xi_0)}{P_n^{m+1^{\circledcirc}}(j\zeta_a)} \right] \right\}. \quad (41)$$

By adding $\bar{H}_d$ to $\bar{H}_v$ given by equations (39), (40), or (41), $\bar{H}$ produced by various dipoles in the oblate spheroid can be calculated. Some representative plots of $\bar{H}$ and $\bar{H}_v$ using a maximum value of $n = 10$ are presented in Fig. 4. As is the case with the prolate spheroid, the ratios of the components of $\bar{H}_d$ and $\bar{H}$ can be calculated for particular locations as required.

Discussion

These results provide a means to investigate and understand the magnetic fields measured near the human body. For example, to a first approximation, the MCG may be considered to be produced by a dipole in a semi-infinite volume and the MEG by a dipole in a sphere. Investigation of the effect of changes in volume conductor shape can then proceed by comparing these fields with those produced by dipoles in prolate and oblate spheroids. The expressions for $\bar{H}$ are in a convenient form to allow an investigation of the relative contribution of $\bar{H}_d$ and $\bar{H}_v$. The infinite series summations in $\bar{H}_v$ for the spheroids present no computational problems when a digital computer is available.

The plot of $\bar{H}$ in Fig. 1B shows that the components of this field tangential to and on the surface of the semi-infinite volume conductor are determined mainly by the dipole at points near the dipole; at distant points they are determined mainly by the current flowing in the volume conductor near that point. (Since H_{zv} is equal to zero, the normal component of $\bar{H}$ is determined completely by the dipole.) This result seems reasonable since $\bar{H}_d$ is greatest directly over the dipole and decreases as $1/R^2$ in moving away from it. Hence, at distant points the field should be determined mainly by the volume current near that point. The change in direction of the field with increasing distance along the x axis clearly shows this change from a primarily dipole to a primarily volume current field. Note that all $\hat{y}$ components of $\bar{H}$ are due solely to the volume current. Comparison of all the plots of $\bar{H}$ and $\bar{H}_v$ in Fig. 1 shows that $\bar{H}_v$ is generally in the direction opposite to $\bar{H}_d$ and therefore tends to cancel it. Recall that the field lines of $\bar{H}_d$ are concentric circles lying in planes perpendicular to the dipole, much like the field lines around an infinitely long straight wire carrying a steady current. The fact that H_{zv} is equal to zero accounts for the parallel field lines in the plots of $\bar{H}_v$ in Figs. 1C and 1D.

For points on the surface of a sphere, the plot of $\bar{H}$ in Fig. 2B shows that the tangential components of this field are determined mainly by the dipole at points near the dipole while at distant points these components are determined mainly by the volume current near that point. This is shown (in larger scale plots) by the field on the negative z axis, which is in the direction opposite to that produced by the dipole alone. As is the case for the semi-infinite volume conductor, the component of $\bar{H}$ normal to the surface is due solely to the dipole. The plot of $\bar{H}$ in Fig. 2C shows the influence of the large current loop flowing in the volume conductor. The plot of $\bar{H}_v$ in Fig. 2B shows that this field is in the direction opposite to $\bar{H}_d$. For points near the dipole, $\bar{H}_v$ is less than $\bar{H}_d$ and therefore $\bar{H}$ is determined mainly by the dipole. The reverse is true for points distant from the dipole. It should be noted that as the dipole is moved closer to the center of the sphere, $\bar{H}$ will decrease because of the increasing cancellation of $\bar{H}_d$ by $\bar{H}_v$. For a dipole at the center of a sphere, complete cancellation of $\bar{H}_d$ by $\bar{H}_v$ will occur. This may be viewed as a special case of the symmetry conditions for which $\bar{H}$ is equal to zero since any dipole at the center of a sphere will be a radial dipole. It should also be noted that since H_{rv} is equal to zero, the field lines of $\bar{H}_v$ in Figs. 2B and 2C are tangential to the surface of the sphere. This is similar to the parallel field lines of $\bar{H}_v$ for the semi-infinite volume.

Study of the plots of $\bar{H}$ in Fig. 3 shows that the tangential components of this field on the surface of a prolate spheroid have the same dependence on distance from dipole location as those for a sphere. Tangential components on the surface of the spheroid and near the dipole are determined mainly by the dipole, while those far from the dipole are determined mainly by the volume current near that point. However, in contrast to the situation which exists for the sphere, the component of $\bar{H}_v$ normal to the surface of the prolate spheroid is not equal to zero over its entire surface. It can be seen from the geometry that the normal component of $\bar{H}_v$ is equal to zero on the z axis. It is also equal to zero on the $z = 0$ plane in Fig. 3B because of the symmetrical distribution of current in relation to this plane for this particular dipole location.

The plots of Fig. 3F show that the component of $\bar{H}_v$ normal to the spheroid surface can become significant in comparison to the same component of $\bar{H}$ for points on the surface distance from the dipole. However, for points near the dipole, this component of $\bar{H}$ is determined mainly by the dipole. The same conclusions can be obtained from a study of the calculated ratios for the normal components of $\bar{H}_d$ and $\bar{H}$ presented in Table 1. Note that the ideal value of this ratio is one which indicates that this component of both $\bar{H}_d$ and $\bar{H}$ are equal and pointing in the same direction. In addition, comparison of the calculated ratios of the normal and tangential components of $\bar{H}_d$ and $\bar{H}$ shows that the normal component of $\bar{H}$ receives the smallest contribution from $\bar{H}_v$. This is clearly shown by the fact that the ratios for the normal component are all positive and have a maximum magnitude of 1.62, while the ratios for the tangential components are negative for most of the locations and have magnitudes greater than 2.00. The negative value of the ratio indicates that this component of $\bar{H}_d$ and $\bar{H}$ are in opposite directions.

A comparison of the plots of $\bar{H}$ in Figs. 3C and 3D shows the increasing contribution of the dipole as it moves close to the surface. The relatively small field produced for the dipole location of Fig. 3C is due to the increased cancellation of $\bar{H}_d$ by $\bar{H}_v$. This degree of cancellation also occurs for other dipoles located near the center of the spheroid and is similar to the situation for a dipole near the center of a sphere.

The previously noted dependence on distance from the dipole is again seen in Fig. 4 for the tangential components of $\bar{H}$ on the surface of an oblate spheroid. As is the case for the prolate spheroid, the normal component of $\bar{H}_v$ is not equal to zero at all points on the surface of the oblate spheroid. This component is, however, equal to zero on the x axis. It is also equal to zero on the $x = 0$ plane in Figs. 4C and 4D because of the symmetrical current distributions in relation to this plane for these dipole locations. The rest of the plots of $\bar{H}_v$ presented in Fig. 4 show that the component of this field normal to the entire spheroid surface is small compared to the same component of $\bar{H}$ for the dipole locations considered. This is in contrast to the situation for the prolate spheroid, where the normal component of $\bar{H}_v$ was significant at points distant from the dipole for some dipole locations. Study of the plots of $\bar{H}$ also show that dipoles near the center tend to produce small $\bar{H}$ (compare Figs. 4C and 4D) because of the increased cancellation of $\bar{H}_d$ by $\bar{H}_v$.

The expressions for $\bar{H}$ and $\bar{H}_v$ as well as the plots of these fields show that for the four volume conductor shapes considered, the component of $\bar{H}$ normal to the surface receives zero or the smallest contribution from the volume current. The normal component of $\bar{H}_v$ is equal to zero for the semi-infinite volume and the sphere; for the spheroids this component is generally small in comparison to the corresponding component of $\bar{H}_d$ but not equal to zero except for certain axes and planes. The plots of $\bar{H}_v$ for the spheroids show that for the dipole locations considered, the normal component of this field on the surface is negligible, except possibly at points distant from the dipole where $\bar{H}$ is small in any event. Exact values for the ratio of the normal components of $\bar{H}_d$ and $\bar{H}$ can be obtained for various dipole and surface locations through the use of the expressions as is done in Table 1. Measurement and use of the normal component of $\bar{H}$ will greatly reduce the complexity of the inverse problem for these four shapes by removing the necessity of considering the field produced by the volume currents. It is important to note that Hosaka *et al.* [8] have found from digital computer model studies of the MCG that the component of $\bar{H}$ normal to a realistic torso surface is the one which receives the smallest contribution from the volume current.

It is important to consider the implications for magnetic measurements of those cases of reduced or zero field produced by dipoles located at or near the center of the volume conductor. This indicates that electrical activity in the center of the head will be difficult to detect with magnetic measurements. Also the zero field produced by dipoles on and oriented along the axis of symmetry of a volume conductor indicates that certain orientations of electrical activity in the head will be difficult to detect with magnetic measurements. Since both these types of electrical activity produce electric potential differences on the surface of the volume conductor, this suggests the possibility of using both electric potential and magnetic field measurements to selectively detect various types of electrical activity in the body. Note that there are various types of electrical activity which will produce large magnetic fields but small electric potential differences [10].

The ability of certain magnetic measurements to detect electrical activity in nerve and muscle tissue with zero or small interference from the current flowing in the volume conductor may also have use in other areas of physiological research. For example, information about the current distribution in a cell membrane might be obtained by measuring the component of $\bar{H}$ normal to a semi-infinite volume (large tank of conducting fluid) containing a cell membrane. Dealing with this component of $\bar{H}$ would reduce the complexity of solving the inverse problem for various assumed models of current distribution in the membrane.

References

[1] D. Cohen and D. McCaughan, "Magnetocardiograms and Their Variation Over the Chest in Normal Subjects," *Amer. J. of Cardiology*, vol. 29, pp. 678–685, 1972.

[2] D. Cohen, H. Hosaka, E. Lepeschin, B. F. Massel, and G. Myers, "Magnetocardiograms of Six Abnormal Subjects and Changes in the Magnetocardiogram of a Normal Subject," accepted for publication in *J. of Electrocardiology*.

[3] J. P. Wikswo, Jr., J. A. Malmivuo, W. H. Barry, G. E. Crawford, W. M. Fairbank, R. P. Giffard, D. C. Harrison, and R. H. Roy, "Vector Magnetocardiography–An Improved Technique for Observation of the Electrical Activity of the Human Heart," *Proceed. of San Diego Biomed. Symp.*, vol. 14, pp. 359–367, 1975.

[4] A. Rosen, and G. T. Inouye, "A Study of the Vector Magnetorcardiographic Waveform," *IEEE Trans. on Biomed. Engr.*, vol. BME-22, pp. 167–174, 1975.

[5] T. J. Teyler, B. N. Cuffin, and D. Cohen, "The Visual Evoked Magnetoencephalogram," *Life Sciences*, vol. 17, pp. 683–691, 1975.

[6] D. Brenner, S. J. Williamson, and L. Kaufman, "Visually Evoked Magnetic Fields of the Human Brain," *Science*, vol. 190, pp. 480–482, 1975.

[7] B. M. Horacek, "Digital Model for Studies in Magnetocardiography," *IEEE Trans. on Mags.*, vol. MAG-9, pp. 440–444, 1973.

[8] H. Hosaka, D. Cohen, B. N. Cuffin, and B. M. Horacek, "The Effect of the Torso Boundaries on the Magnetocardiogram," accepted for publication in *J. of Electrocardiology*.

[9] B. N. Cuffin, "Model Studies of Electrocardiograms and Magnetocardiograms Using Realistic Torso Boundaries," Ph.D. Dissertation, The Pennsylvania State University, 1974.

[10] D. Cohen, and H. Hosaka, "Magnetic Field Produced by a Current Dipole," Accepted for publication in *J. of Electrocardiology*.

[11] F. Grynszpan, and D. B. Geselowitz, "Model Studies of the Magnetocardiogram," *Biophys. J.*, vol. 13, pp. 911–925, 1973.

[12] D. B. Geselowitz, "On the Magnetic Field Generated Outside an Inhomogeneous Volume Conductor by Internal Current Sources," *IEEE Trans. on Mags.*, vol. MAG-6, pp. 346–347, 1970.

[13] G. A. Campbell, and R. M. Foster, *Fourier Integrals for Practical Applications*, D. Van Nostrand Co., Inc., 1948, pg. 126.

[14] *ibid.*, pg. 111.

[15] F. Grynszpan, "Relationship Between the Surface Electromagnetic Fields and the Electrical Activity of the Heart," Ph.D. Dissertation, University of Pennsylvania, 1971, pg. 26.

[16] P. M. Berry, "*N, M* Space Harmonics of the Oblate Spheroid," *Annals of N.Y. Acad. of Sciences*, vol. 65, pp. 1126–1134, 1956.

[17] W. R. Smythe, *Static and Dynamic Electricity*, 3rd. ed., McGraw-Hill Book Co., 1968, pg. 210.

[18] *Tables of Associated Legendre Functions*, National Bureau of Standards, Columbia University Press, 1945.

[19] Smythe, *Static and Dynamic Electricity*, pg. 166.